

Article

Investigation of Possible Leaching Control Mechanisms for Chromium and Vanadium in Electric Arc Furnace (EAF) Slags Using Combined Experimental and Modeling Approaches

Simone Neuhold ^{1,*}, André van Zomeren ², Joris J. Dijkstra ³ , Hans A. van der Sloot ⁴, Peter Drissen ⁵, David Algermissen ⁵, Dirk Mudersbach ⁶, Susanne Schüler ⁶, Thomas Griessacher ⁷, Johann G. Raith ⁸ , Roland Pomberger ¹ and Daniel Vollprecht ¹ 

¹ Chair of Waste Processing and Waste Management, Montanuniversitaet Leoben, Franz-Josef-Straße 18, 8700 Leoben, Austria

² Energy Research Centre of the Netherlands (ECN) part of TNO, Westerduinweg 3, 1755 ZG Petten, The Netherlands

³ Netherlands Organisation for Applied Scientific Research (TNO) Geological Survey of the Netherlands, Princetonlaan 6, 3584 CB Utrecht, The Netherlands

⁴ Hans van der Sloot Consultancy, Glenn Millerhof 29, 1628 TS Hoorn, The Netherlands

⁵ FEHS Building Materials Institute, Bliersheimer Straße 62, 47229 Duisburg, Germany

⁶ Max Aicher Umwelt GmbH, Industriestraße 1, 86405 Meitingen, Germany

⁷ Stahl- und Walzwerk Marienhütte GmbH, Südbahnstraße 11, 8021 Graz, Austria

⁸ Chair of Resource Mineralogy, Montanuniversitaet Leoben, Peter-Tunner-Straße 5, 8700 Leoben, Austria

* Correspondence: simone.neuhold@unileoben.ac.at; Tel.: +43-3842-402-5133

Received: 31 July 2019; Accepted: 27 August 2019; Published: 30 August 2019



Abstract: In this study, possible leaching control mechanisms for Cr and V in electric arc furnace slags were investigated by using a multi-methodological approach. Aside from chemical and mineralogical bulk analyses, special emphasis was given to surface investigations of the slags prior to and after leaching. In addition, pH dependence leaching tests were performed and the obtained data were evaluated with hydrogeochemical models. Investigations revealed that Cr and V are mainly bound in spinel and wuestite as well as minor amounts of olivine. Spinel and wuestite do not dissolve during water leaching for 48 h, whereas, depending on the composition of olivine, this phase either dissolves and releases V and Cr congruently, or does not dissolve but may hydrate. Melilite may also hydrate, but neither V nor Cr were detected in this phase. It appears that leached V is subsequently adsorbed onto these newly hydrated phases. The combination of the applied methods further showed that the abundance of calcium silicates, spinel, and wuestite is influenced by the FeO/SiO₂ and CaO/SiO₂ ratio in the slag. Therefore, it is assumed that the leaching of V and Cr can be minimized by changing these ratios to favor the formation of Fe bearing calcium silicate and spinel instead of wuestite.

Keywords: electric arc furnace slag; mineralogical characterization; leaching mechanism; vanadium; chromium; geochemical modeling

1. Introduction

In Austria, up to 100 million tons of natural rocks are mined as raw materials for building and construction purposes every year, yielding a consumption of approximately 12 tons per capita a year, which is twice as high as the average consumption in the European Union (with the exceptions of Finland, Romania, and Estonia). Additionally, 2.5 million tons of ore are mined per year for steelmaking industries; however, the major part of the almost 10 million tons required has to be imported [1].

During the steel making process, approximately 2.5 million tons per year of blast furnace (BF) slags and steel slags accrue in Austria [2], of which 78,000 tons per year arise from electric arc furnaces (EAF) [3]. Using EAF slag as a building material, for example, in road construction [4–7], not only leads to the conservation of natural raw materials, but it also supports circular economy aspects, because recycled steel products, or scrap, are used as the input material instead of primary ore as in the BF. However, a use is of course only possible, if no environmental risks emanate from EAF slags.

Slag serves as an essential metallurgical instrument during the steelmaking process to ensure the quality of the steel. Elements such as Si, which have negative effects on the quality of the steel, are withdrawn by adding slag forming compounds such as CaO and MgO [8]. Depending on the steelmaking process, the main elements in the slags are Si, Ca, Mg, and Al as well as Fe. Additionally, minor amounts of alloying elements that are necessary to enhance the steel quality can be incorporated in the slag, which originates from recycled scrap or from secondary metallurgy. Some of these elements, like V and Cr, can pose environmental risks if leached from the slags [9,10]. However, particularly in the case of Cr, the oxidation state is crucial, since Cr(III) is considered to be an essential trace element for the human metabolism, whereas Cr(VI) is carcinogenic [11,12]. In the case of V, the oxidation state also has to be considered because the toxicity of V increases with increasing valency [13–15]. For basic oxygen furnace (BOF) slags, Chaurand et al. [16,17] showed that in powder samples, Cr is present as Cr(III) prior to and after water leaching and that V is predominately present as V(IV) and increases its oxidation state to V(V) during ageing. Hobson et al. [18] also showed that V was released as V(V) from dicalcium silicates in BOF slags. To our knowledge, no analogous information is available for EAF slags. Attempts to determine the oxidation state of Cr and V in single mineral grains in the original slag samples and after being exposed to water for 48 h are described in Neuhold et al. [19].

To minimize a potential risk evolving from leaching of the alloying elements V and Cr, several investigations on slags have been published. These studies reveal that the leaching is controlled by the mineralogy of the slags in three main ways: through the stability of the primary mineral phases; the formation of secondary mineral phases; and adsorption onto mineral surfaces. Subsequently, leached ions may be immobilized due to the sorption properties of the matrix, for example, soil [20,21]. For Cr, binding in the spinel crystal structure and the low solubility of the spinel phase was identified as the leaching control mechanism (e.g., [22,23]). Strandkvist et al. [24,25] described the incorporation of Cr₂O₃ in magnesiowuestite and the dependence of Cr leaching on the amount of FeO present, stating that higher amounts of FeO in the grain led to lower Cr leaching. The incorporation of V in spinel and brownmillerite in EAF slags was shown by Mombelli et al. [26] and its binding in calcium silicates such as larnite in BOF slags by van Zomeren et al. [27] and Drissen [28,29]. These studies indicate the influence of the chemical composition on the mineral composition and consequently on the leaching behavior. Higher Cr₂O₃, MgO, and Al₂O₃ contents enhance the formation of spinel and the addition of SiO₂ promotes the formation of gehlenite (instead of brownmillerite), both leading to a decrease in the leaching of Cr and V, respectively [24–26,30,31]. Other studies have stated that secondary mechanisms such as the precipitation of calcium silicate hydrates (CSH) and Ca vanadates control the leaching behavior of V [18]. In contrast, Loncnar et al. [32] postulated that the leaching was mainly controlled by surface reactions and not by the chemical composition of the investigated ladle slags. These contradictory results demonstrate that the exact controlling mechanisms for the mobility of Cr and V in slags are not completely understood yet. Therefore, in this study, hydrogeochemical modeling and experimental methods, with special emphasis given to surface analyses before and after leaching tests, were used to investigate these complex connections between slag properties and leaching behavior. Not all of the above-mentioned mechanisms were confirmed, but new possible leaching control mechanisms were identified for Cr and V.

The findings of this study can be used as a basis to further develop an environmentally safe utilization of EAF slags as construction materials by tailoring the slag properties during the steelmaking process to minimize the leaching of Cr and V.

2. Materials and Methods

2.1. Samples

In this study, five EAF slag samples from two different steel plants were analyzed. Slag sample EAFS1 represents the standard operating conditions of steel plant 1 and was sampled according to ÖNORM S 2127 [33] by taking ten representative subsamples of 36 kg from one steel charge, adding up to a total of 360 kg. These subsamples were characterized (see Section 2.2) individually and as a collective sample. The other four samples (of 20 kg) were taken at steel plant 2. Two of these slag samples (EAFS2_1 and EAFS2_2) were generated by the standard procedure of the steel plant, but with different formation times (beginning/not reduced and tapping/reduced) and different cooling rates: since the melt is poured in a slag pot, sample EAFS2_1 represents a comparably slow cooling rate (cooled in the center) and sample EAFS2_2 represents a comparably fast cooling rate (cooled at the pot wall). The other two slag samples were conditioned with varying additives (internal procedure of the steel plant) during the steelmaking process (EAFS2_A and EAFS2_B).

2.2. Methods

2.2.1. Chemical Characterization

All samples were crushed (jaw crusher, Retsch BB 200, Retsch GmbH, Haan, Germany), ground (ball mill, Retsch S 1000, Retsch GmbH, Haan, Germany), and dried at 105 ± 3 °C (drying oven, according to DIN EN 14346 [34]) prior to microwave digestion with a mixture of HF, HNO₃, and HCl according to ÖNORM EN 13656 [35]. The chemical composition of all EAF slag samples was determined by using an inductively coupled plasma mass spectrometry (ICP-MS) system from Agilent Type 7500 (Agilent Technologies, Inc., Santa Clara, CA, USA) for cation concentrations (according to ÖNORM EN ISO 17294-2 [36]) and by using inductively coupled plasma optical emission spectrometry (ICP-OES, Varian Vista-MPX CCD Simultaneous System, 4.1.0, Agilent Technologies, Inc., Santa Clara, CA, USA) for the sulfur concentrations. To determine the fluorine concentrations, an alkaline digestion using NaHCO₃ and Na₂CO₃, according to [37], was performed prior to ion chromatography (IC, Dionex ICS-2000). Hexavalent Cr was determined according to DIN 38405-24/EPA method 3060 A [38] by using a UV/VIS spectrometer (UNICAM UV4). All analyses were conducted at the Chair of Waste Processing Technology and Waste Management of the Montanuniversität Leoben.

The oxidation states of Cr and V in single mineral grains were investigated for fresh and leached polished sections via x-ray absorption near-edge spectroscopy (XANES) for samples EAFS1 and EAFS2_1. The water free preparation of the polished sections is described in detail in Neuhold et al. [19]. Leaching of the polished sections is described in Section 2.2.3. For each sample, two polished sections (mirror image) were prepared to analyze the surface prior to and after leaching during one beamtime at the μ Spot beamline at the electron storage ring BESSY II in Berlin-Adlershof of the Helmholtz Center Berlin for Materials and Energy. Twelve measuring spots (three grains per mineral phase) were selected per sample (for details see Neuhold et al. [19]). The measuring spots were excited with x-rays, 50 eV below and 150 eV above the K absorption edge of Cr (5.989 keV) and V (5.465 keV), covering a range of 200 eV. The following standards were used: Cr₂O₃, MgCr₂O₄, Cr(OH)₃, CaCr₂O₄, FeCr₂O₄, CaCrO₄, BaCrO₄, K₂CrO₄, FeV₂O₄, VO, VO₂, and V₂O₅.

2.2.2. Mineralogical Characterization

X-ray diffraction (XRD) measurements were conducted for all described samples with a PANalytical X'Pert Pro instrument (PANalytical B.V., Almelo, The Netherlands) at the Institute of Applied Geosciences of Graz University of Technology. The data were collected using Co-K α radiation at 40 mA and 45 kV. The samples were rotated and data points were recorded for a 2θ angle between 4° and 85° with a step size of 0.008°.

The surface of the fresh and leached (see Section 2.2.3) samples was characterized with the electron microprobe (EMP) technique using the Superprobe JEOL JXA 8200 (JEOL Ltd., Akishima, Japan) at the Chair of Resource Mineralogy of Montanuniversitaet Leoben. Quantitative analyses were recorded in wavelength dispersive spectrometer (WDS) mode by using the $K\alpha$ lines of Ca, Mg, Mn, Si, Al, Fe, V, Cr, Mo, and F. The following spectrometer crystal arrangement was selected: TAP for Mg, Al and F, PETJ for Si, Ca, Mo, and LIFH for V, Cr, Mn, and Fe. The instrument was calibrated with the following standards: chromite, chromium(III) oxide, wollastonite, diopside, and kaersutite. The instrument was operated with an acceleration voltage of 15 kV and a beam current of 10 nA. The detection limits for the quantitative analyses ranged between 0.023 and 0.053 mass-% for V and 0.027 to 0.037 mass-% for Cr and were considered separately for every measuring set during data evaluation (see Tables S1–S14).

2.2.3. Leaching Experiments

The pH dependence leaching tests were conducted according to EN 14429 [39] for 48 h with a liquid to solid (L/S) ratio of 10. The samples were crushed to a grain size <1 mm and the acid neutralization capacity as well as the base neutralization capacity were determined. Afterward, eight leaching experiments were performed per sample: one with distilled water (= natural pH) and seven by adding the necessary amounts of HNO₃ and NaOH, respectively, to reach final pH values after 48 h from pH 2 to 13 (with a maximum interval of 1.5 pH units). The pH was measured after 4 h, 44 h, and 48 h and the maximum pH change between 44 h and 48 h did not exceed 0.3 pH units. After filtration with a membrane filter (pore size 0.45 μ m) the leachates were analyzed using ICP-MS, ICP-OES, IC, and photometrically, as described in Section 2.2.1.

The polished sections were leached by stirring from underneath on the basis of ÖNORM S 2116-4 [40] in distilled water for 48 h (instead of 24 h). The L/S ratio could not be determined exactly because the samples were already embedded in epoxy resin. However, the leachates were not further considered, since these leaching tests were solely performed to investigate surface changes.

2.2.4. Hydrogeochemical Modeling

Hydrogeochemical modeling was performed using the software LeachXSTM/Orchestra version 2.0.90 (ECN, DHI, Vanderbilt University, Nashville, TN, USA). The pH dependence leaching tests served as input data by determining the maximum concentration at pH values between 1 and 14 (availability) for each element. The concentrations for 23 elements (19 cations and four anions) were implemented. The input amount of CO₃²⁻ in the model is difficult to estimate as the degassing of CO₂ occurs at low pH, while CO₂ is adsorbed by the suspension at high pH [41]. Therefore, the input amount of CO₃²⁻ was estimated for each sample via trial and error by adjusting the calculated concentrations of Ca compared to the experimentally determined concentrations. Additionally, the values for hydrous ferric oxides (HFO) as a specific adsorbing surface were determined for samples EAFS1 and EAFS2_1 via ascorbate, dithionite (both according to Kostka and Luther [42]) and oxalate (according to Blakemore et al. [43]) extraction. These experiments were conducted by the Energy Research Centre of the Netherlands (ECN, now ECN part of TNO). For the other samples, the HFO amount was used as a model calibration parameter. The L/S ratio was set to 10 in the model, according to the performed leaching experiments and the sum of pe and pH was set to 10. A lower sum of pe and pH compared to the experimental data (12 to 13) was used because a better fit for Fe was achieved, being in good agreement with the mineralogical characterizations where Fe(II) is the predominant valence state for Fe in the investigated EAF slags (see Section 3). The thermodynamic database minteq.v4.dat was used as the basis for the calculations. To cover various possible precipitation and adsorption reactions, described as leaching control mechanisms in the literature (see Section 1), further information was implemented via database extensions (patches). Those patches (created by Dijkstra and Meeussen and Vollprecht and Neuhold) contained mineral phases from the literature, the thermodynamic database llnl.dat (Lawrence Livermore National Laboratory), and the adsorption model according to Dzombak and Morel [44]. Solid solutions (e.g., a spinel solid solution with the end members FeCr₂O₄,

MgCr₂O₄, MgAl₂O₄, FeAl₂O₄, Mn₃O₄, and FeV₂O₄) were implemented according to Meeussen (2014, Standard ORCHESTRA object definitions Version 2014). By comparing the experimental data to the thermodynamic calculations provided by the model, a set of 184 mineral phases, six solid solutions, and adsorption onto HFOs was selected from the compiled database. Precipitation reactions were suppressed for mineral phases that were unlikely to occur in slag systems and that underestimated the experimentally determined leached concentrations by orders of magnitude. For detailed information regarding the input data, model components, and modeled results for the elements (Ca, Si, Fe, Al, Mg and Mn), see Supplementary Material Tables S15–S22 and Figure S1.

3. Results

3.1. Chemical and Mineralogical Composition

Table 1 shows the bulk concentrations of selected elements (concentration > 1 mass-%) and V in the investigated EAF slags. Major elements were Ca and Fe. The concentrations for Cr_{total} were around 1 mass-%, however, the measured Cr(VI) concentrations were very low. Vanadium concentrations were around 0.1 mass-%.

Table 1. Bulk chemical composition (in mass-%) of the investigated EAF slags. Non-conditioned: samples from standard procedure; conditioned: samples with additives (internal steel plant procedure); (s = 1σ).

Total Content (Mass-%)	Non-Conditioned Samples			Conditioned Samples	
	EAFS1 n = 10	EAFS2_1 n = 2	EAFS2_2 n = 2	EAFS2_A n = 1	EAFS2_B n = 2
Ca	15.1 ± 1.6	27.5 ± 0.4	28.1 ± 0.4	16.6	16.9 ± 0.6
Si	4.9 ± 0.3	7.8 ± 0.2	6.7 ± 0.9	8.9	11.7 ± 0.3
Fe	29.6 ± 1.4	20.6 ± 0.5	21.8 ± 1.3	22.8	20.3 ± 2.5
Al	3.9 ± 0.4	3.0 ± 0.3	3.1 ± 0.2	2.2	4.8 ± 0.03
Mn	3.6 ± 0.2	5.0 ± 0.3	5.9 ± 0.1	3.1	4.2 ± 0.06
Mg	3.7 ± 1.4	3.3 ± 0.3	3.0 ± 0.3	2.3	2.4 ± 0.04
Cr _{tot}	1.2 ± 0.1	0.98 ± 0.05	0.91 ± 0.3	1.2	1.5 ± 0.06
V	0.07 ± 0.01	0.09 ± 0.01	0.10 ± 0.002	0.09	0.11 ± 0.02
Cr(VI)	< 2.0 × 10 ⁻⁴	2.4 × 10 ⁻⁵ ± 0.00	2.4 × 10 ⁻⁵ ± 1.1 × 10 ⁻⁵	1.6 × 10 ⁻⁵	1.8 × 10 ⁻⁵ ± 8.5 × 10 ⁻⁶

Results for the bulk mineralogy (for the XRD results, see Supplementary Material Figure S2 and Table S23) and the microprobe analyses are summarized in Table 2. Results of the mineral chemical analyses are listed in Tables S1–S14. Two of the five presented samples showed a similar mineralogical composition, but varying mineral chemical compositions of the phases due to solid solutions: a wuestite solid solution (Fe,Mg,Mn)O, a spinel solid solution AB₂O₄ (with A = Fe, Mg, Mn and B = Al, Cr, Fe, Mn), an olivine group phase A₂SiO₄ (with A = Ca, Fe, Mg, Mn), and a melilite group phase Ca₂M(XSiO₇) (with M = Mg, Fe, Al and X = Si, Al). The olivine group phase included: fayalite (Fe₂SiO₄), forsterite (Mg₂SiO₄), tephroite (Mn₂SiO₄), glaucocroite (CaMnSiO₄), kirschsteinite (CaFeSiO₄), monticellite (CaMgSiO₄), and calcio-olivine (γ-Ca₂SiO₄) [45] as well as larnite (β-Ca₂SiO₄) and bredigite ((Ca₁₄Mg₂(SiO₄)₈) and every solid solution between these end members. The end members åkermanite (Ca₂Mg(Si₂O₇)), gehlenite (Ca₂Al(AlSiO₇)), and ferri-gehlenite (Ca₂Fe(AlSiO₇)) or any solid solution among these end members can be summarized as the melilite group phase.

Table 2. Mineral phases (determined by XRD) and calculated mean stoichiometric composition of the measured phases (from the EMP analyses) of the investigated EAF slag samples. All Fe and Mn were calculated as Fe²⁺ and Mn²⁺. Italics indicate phases with very low signal in the diffractogram.

Sample	XRD	EMPA	Abbreviation	
	Mineral Phases	Calculated Stoichiometry	Analyses	
EAFS1	Spinel	(Mg _{0.5} Fe _{0.6} Mn _{0.1})(Cr _{1.0} Al _{0.9})O ₄	5	Spl
	Wuestite	(Fe _{0.8} Mn _{0.1} Mg _{0.1})O	10	Wus
	Gehlenite	Ca ₂ (Mg _{0.2} Fe _{0.2} Al _{1.3})Si _{1.3} O ₇	5	Mll
	Monticellite	(Ca _{1.2} Mg _{0.2} Fe _{0.5} Mn _{0.2})SiO ₄	5	OI1
EAFS2_1	<i>Spinel</i>	(Mg _{0.6} Fe _{0.4} Mn _{0.2})(Cr _{1.6} Al _{0.3})O ₄	5	Spl
	Wuestite	(Fe _{0.6} Mn _{0.2} Mg _{0.2})O	10	Wus
	Bredigite	(Ca _{1.9} Mg _{0.1})SiO ₄	10	OI2
	Wuestite	(Fe _{0.7} Mn _{0.2} Mg _{0.1})O	10	Wus
EAFS2_2	Åkermanite	Ca ₂ (Mg _{0.1} Fe _{0.1} Al _{1.6})Si _{1.2} O ₇	6	Mll
	Bredigite	(Ca _{1.7} Mg _{0.2} Fe _{0.1})SiO ₄	6	OI2
	-	Ca-Si-Ti-Fe (by EDS)	3	T
	<i>Spinel</i>	(Mg _{0.3} Fe _{0.7} Mn _{0.1})(Cr _{1.5} Al _{0.5})O ₄	13	Spl
EAFS2_A	Wuestite	(Fe _{0.7} Mg _{0.1} Mn _{0.1})O	10	Wus
	Gehlenite	Ca _{1.9} (Mg _{0.2} Fe _{0.2} Al _{1.2})Si _{1.4} O ₇	10	Mll
	Kirschsteinite	(CaMg _{0.3} Fe _{0.5} Mn _{0.1})SiO ₄	13	OI1
	Bredigite	(Ca _{1.8} Mg _{0.1} Fe _{0.1})SiO ₄	3	OI2
	<i>Spinel</i>	(Mg _{0.4} Fe _{0.5} Mn _{0.2})(Cr _{1.2} Al _{0.8})O ₄	14	Spl
EAFS2_B	Wuestite	grains < 10 µm	-	Wus
	Gehlenite	Ca _{1.9} (Mg _{0.3} Fe _{0.2} Al _{1.1})Si _{1.5} O ₇	10	Mll
	Kirschsteinite	(Ca _{0.9} Mg _{0.2} Mn _{0.3} Fe _{0.6})Si _{1.0} O ₄	10	OI1

Table 3. Mean concentrations of Cr and V of all measured phases (see Table 2) before (BL) and after leaching (AL) for spinel solid solutions (Spl), wuestite solid solutions (Wus), melilite group phases (Mll), and olivine group phases (Ol); ($s = 1\sigma$). Abbreviations: no analyzed grain (-), below detection limit (b.d.), and dissolved (d). Results of the chemical mineral analyses of single grains are listed in Tables S1–S14.

Phase	EAFS1		EAFS2_1		EAFS2_2		EAFS2_A		EAFS2_B	
	BL	AL								
Chromium (mass-%)										
Spl	26.3 ± 2.0	24.2 ± 3.6	40.8 ± 2.0	40.5 ± 2.1	-	38.7 ± 2.3	34.7 ± 4.3	36.6 ± 6.0	28.5 ± 3.9	28.2 ± 4.1
Wus	0.67 ± 0.20	0.74 ± 0.20	1.54 ± 0.32	1.44 ± 0.44	0.96 ± 0.14	0.96 ± 0.27	2.59 ± 2.2	3.50 ± 2.0	<10 µm	<10 µm
Mll	b.d.	0.07 ± 0.03	-	-	b.d.	0.05 ± 0.01	b.d.	b.d.	b.d.	b.d.
Ol1	b.d.	0.05 ± 0.03	-	-	-	-	b.d.	0.08 ± 0.08	b.d.	b.d.
Ol2	-	-	b.d.	d	b.d.	d	0.04 ± 0.02	d	-	-
Vanadium (mass-%)										
Spl	0.12 ± 0.05	0.14 ± 0.03	0.10 ± 0.04	0.07 ± 0.02	-	0.08 ± 0.03	0.07 ± 0.03	0.19 ± 0.10	0.12 ± 0.04	0.19 ± 0.10
Wus	0.05 ± 0.02	0.09 ± 0.05	b.d.	b.d.	0.09 ± 0.03	0.06 ± 0.02	0.07 ± 0.03	0.16 ± 0.06	<10 µm	<10 µm
Mll	b.d.	b.d.	-	-	b.d.	b.d.	b.d.	b.d.	b.d.	b.d.
Ol1	b.d.	b.d.	-	-	-	-	b.d.	b.d.	b.d.	b.d.
Ol2	-	-	0.06 ± 0.03	d	b.d.	d	b.d.	d	-	-

In sample EAFS2_1, no melilite was detected and the olivine group phase lacked Fe and Mn. No spinels were found in sample EAFS2_2 and an olivine group phase without Mn was formed. In sample EAFS2_A, an additional olivine group phase was found, again with no Mn present. EMP analyses revealed higher stoichiometric variations for olivine when compared to the other phases. Aside from oxides (spinel and wuestite) and calcium silicate phases (olivine and melilite), metallic inclusions were found in all samples. Regarding Cr and V, the results in Table 2 revealed that Cr was bound in chromium-rich spinel group phases, but no discrete V bearing phase was found. However, Table 3 shows that V and Cr were present as trace elements in almost all other phases. Vanadium was mainly incorporated in spinel and wuestite solid solutions and also in the olivine phase in sample EAFS2_1. Besides the binding of Cr in the spinel phases, Cr could also be incorporated in the wuestite lattice and, in sample EAFS2_A, in minor amounts in one of the olivine phases (see Table 3). Neither V nor Cr were detected in the melilite group phase in any of the samples. XANES measurements revealed that Cr was bound as Cr(III) in the spinel and wuestite phases and V was bound as V(III) in the spinel (Neuhold et al. [19]). No Cr(VI) was found, either in the fresh or leached samples.

3.2. Qualitative and Quantitative Surface Investigations

Comparison of the fresh and leached surface of the slag samples (Figure 1) showed that the spinel, wuestite, and melilite phases did not dissolve after being exposed to water for 48 h in all samples. However, possible hydration reactions during the leaching of melilite and olivine group minerals were assumed because the quantitative analyses of some of these phases did not add up to 100% after leaching (see Tables S1–S14). The olivine phases dissolved completely in some samples, depending on the amount of Mn, Fe, and Ca present in the phase (Figure 1 and Table 2); higher Mn and Fe content and a lower Ca content enhanced the stability of this phase. Due to the roughness of the sample surface after the leaching, the quantitative analysis was restricted for some grains and the analyses showed significant standard deviations. However, in general, incorporation of Cr and V in the spinel via cationic substitution seemed to be favorable for both elements when compared to their incorporation in olivine and wuestite phases. V and Cr may leach from olivine if it dissolves during leaching, and wuestite only incorporates limited amounts of Cr and V in its structure [25].

The differences in Cr concentrations in the investigated spinel grains (Table 3) prior to and after water leaching for 48 h were within the range of standard deviations for the measurement, hence, no significant decrease due to leaching was detected. The change in Cr concentrations in single wuestite grains after leaching could only be evaluated in samples EAFS1 and EAFS2_1, respectively EAFS2_2. In sample EAFS2_A, the standard deviation of the measurements was in the range of the determined mean concentration and in sample EAFS2_B, no quantitative analysis could be performed on wuestite because the grain size of the phase was below 10 μm . After considering the mean concentrations and standard deviations, it can be deduced that Cr is bound, comparably stable, in both wuestite and spinel. A high FeO content above 65 mass-% in the investigated wuestite prevented Cr leaching [25] (see Tables S1–S14). However, the absolute Cr concentrations in the investigated spinel and wuestite phases were quite different. Spinel compositions were close to the chromian end members, corresponding to Cr concentrations up to 40 mass-% per grain, whereas Cr was incorporated in the wuestite structure only in traces, with up to 3 mass-% per grain. Chromium concentrations in the analyzed calcium silicate phases were below or close to the detection limit and have to be evaluated with caution due to the high standard deviations up to 100%. Nevertheless, in sample EAFS2_A, the olivine phase (Ol2) dissolved during water leaching for 48 h, therefore, it can be assumed that the incorporated Cr was released.

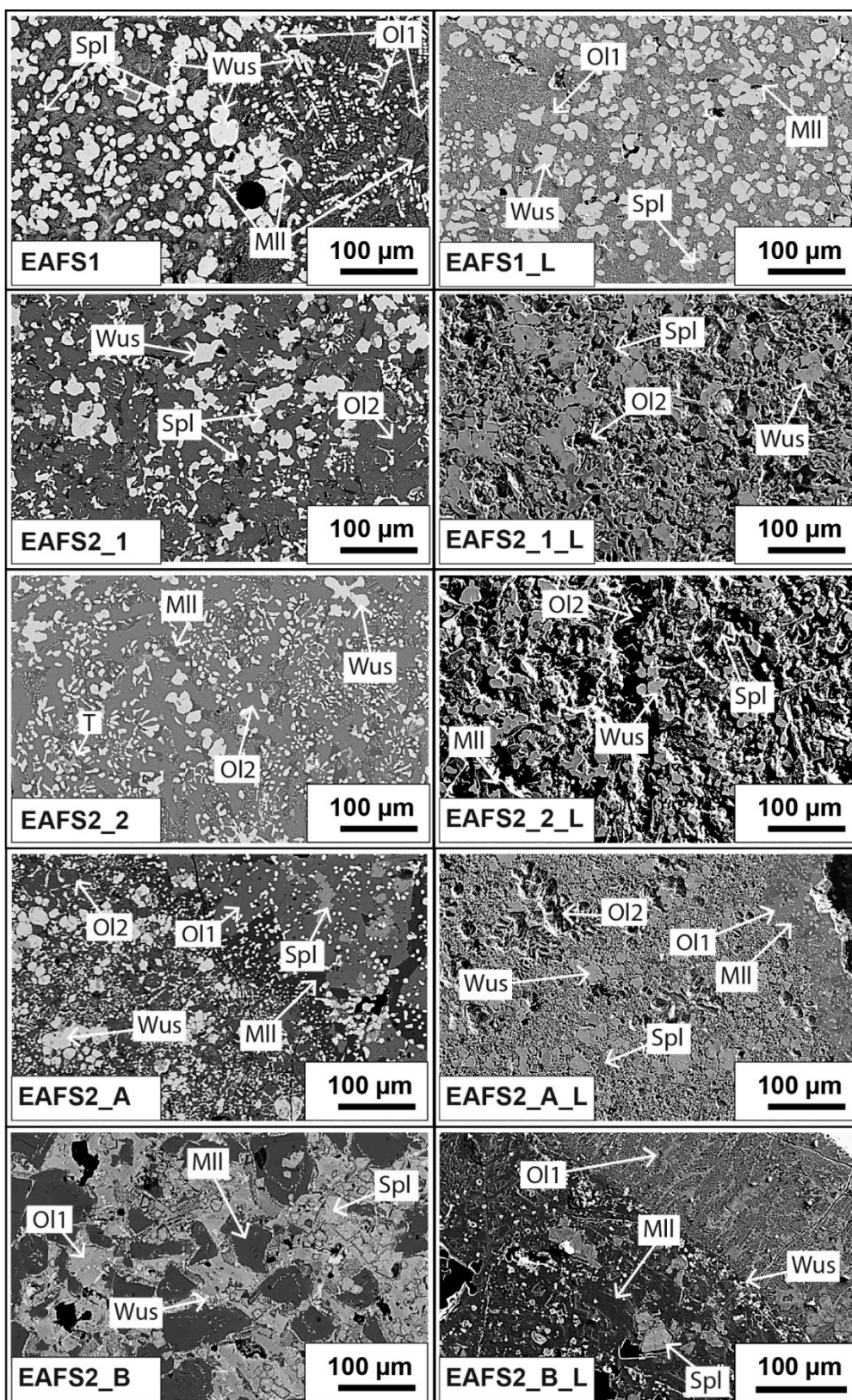


Figure 1. Electron images of five EAF slag samples taken by EMP. **(Left)** Backscattered electron (BSE) images before leaching. **(Right)** Secondary electron (SE) images after leaching. Abbreviations: wuestite (Wus), spinel (Spl), olivine (Ol), melilite (Mll), and Ca-Ti-phase (T).

The concentrations of V in the single grains prior to and after leaching did not differ significantly, neither in spinel nor in wuestite, after taking the elevated standard deviations for the measurements after leaching (up to 50%) into account. Similar low V concentrations (close to the detection limit) were present in wuestite and spinel. Exceptions are sample EAFS2_1, where no V was detected in wuestite but in spinel, and sample EAFS2_B, where the wuestite crystals were too small for quantitative analyses. In all analyzed calcium silicate phases (except sample EAFS2_1), the V concentrations were below the detection limit. In sample EAFS2_1, V was released due to the dissolution of the V bearing olivine phase.

3.3. Modeling Results

The results of the pH dependence leaching tests combined with those of thermodynamic modeling are shown in Figure 2 for the non-conditioned samples (EAFS1, EAFS2_1, and EAFS2_2) and in Figure 3 for the conditioned samples (EAFS2_A and EAFS2_B). Although the total and the leached concentrations of Cr and V differed (Tables 1 and 4) for all of the presented samples, the same specific leaching trends, meaning the leaching behavior over the pH range from 2 to 14, was observed for Cr and V, respectively, in all samples. The experimental concentrations for leached Cr showed the highest concentration at pH 2 and a continuous decrease up to pH 5. Between pH 5 and pH 10/11, the concentrations remained low at around 0.01 mg/kg DM and below, and increased toward higher pH values, but did not exceed the maximum concentrations at low pH values. In the pH range from 9 to 13, higher concentrations of Cr were released from sample EAFS1 than from the other samples. For environmental evaluations, the pH domain between natural pH (around 11) and expected lower pH values (around 8) for fully weathered samples are the most relevant.

The concentrations of leached V decreased significantly from pH 2 to approximately 6, followed by an increase to natural pH (10.8–11.2). Between pH 11 and 14, the concentrations slightly decreased. According to the modeled results for the pH-dependent leaching behavior of the non-conditioned slag samples (Figure 2), Cr leaching might be controlled by two primary mineral phases: a Cr-spinel solid solution in the range of the natural pH and a wuestite solid solution also in the range of the natural pH (except for sample EAFS1) and at a lower pH. Additionally, a secondary mineral phase $\text{Ba}(\text{S,Cr})\text{O}_4(96\%\text{SO}_4)$ (data implemented from Rai et al. [46]) might precipitate over a large pH range and adsorption onto HFOs is suggested as the controlling mechanism. For the conditioned samples (Figure 3), the same controlling mechanisms were calculated, except for sample EAFS2_A, where no wuestite solid solution was predicted to form. According to the results from the thermodynamic model, the leaching of V is mainly controlled by adsorption onto HFOs and at lower pH by the precipitation of Fe vanadate (Figures 2 and 3). For all non-conditioned samples, in addition to the predominant species $\text{Fe}(\text{VO}_3)_2$, the wuestite solid solution may precipitate at pH 4–6. For sample EAFS1, an ettringite solid solution was calculated to subordinately control the leaching in the natural pH range (see Supplementary Material Figure S3).

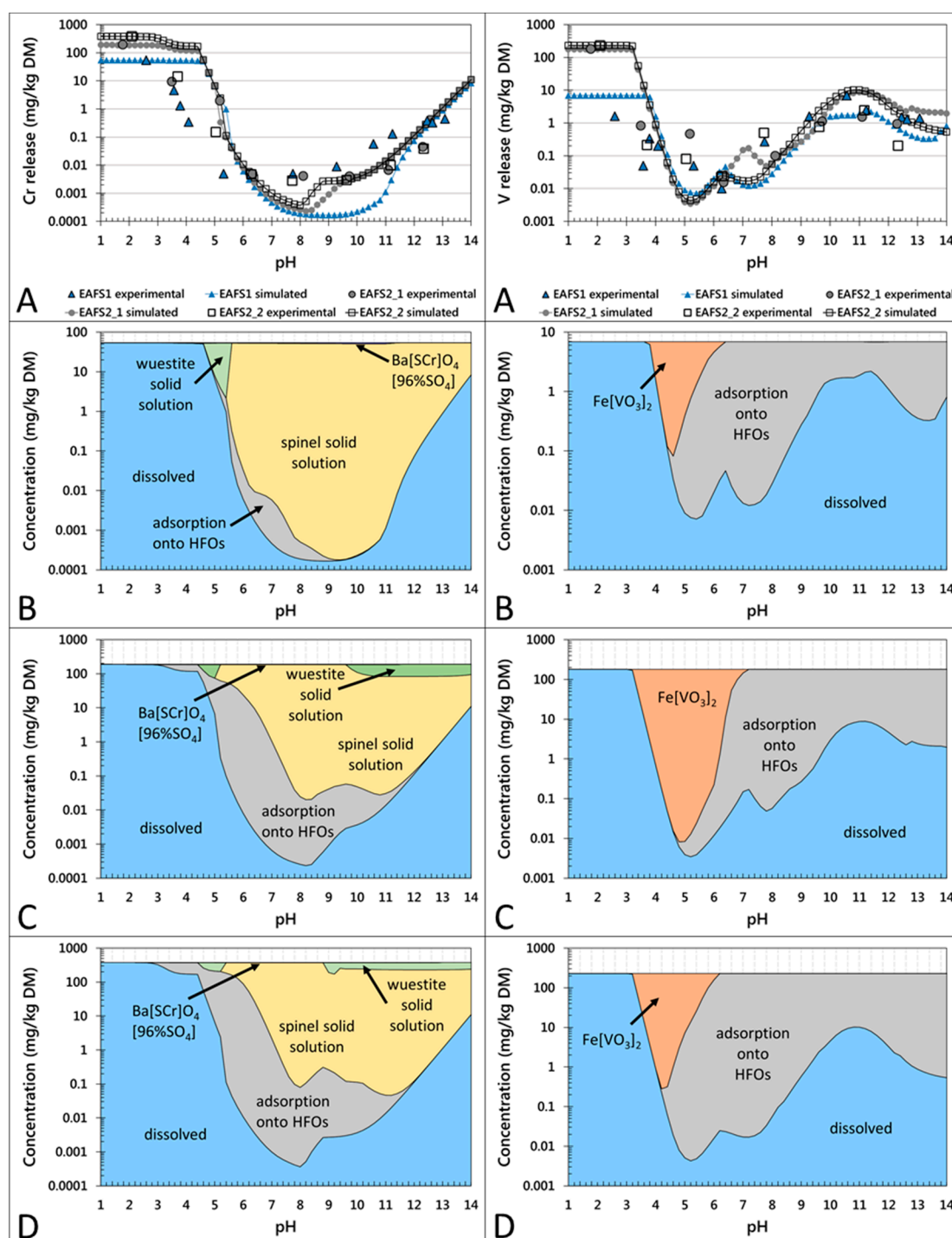


Figure 2. pH-dependent leaching behavior of Cr (left column) and V (right column) in the non-conditioned EAF slag samples EAFS1, EAFS2_1, and EAFS2_2. Partitioning in the solution (A) and in the solid (B–D) are given on a weight basis. (A) Experimentally determined release of Cr and V, respectively (larger symbols without line) and calculated results with LeachXS™/Orchestra (corresponding symbols with lines). (B–D) Calculated concentrations of leaching control phases/mechanisms for Cr and V, respectively in samples EAFS1 (B), EAFS2_1 (C), and EAFS2_2 (D).

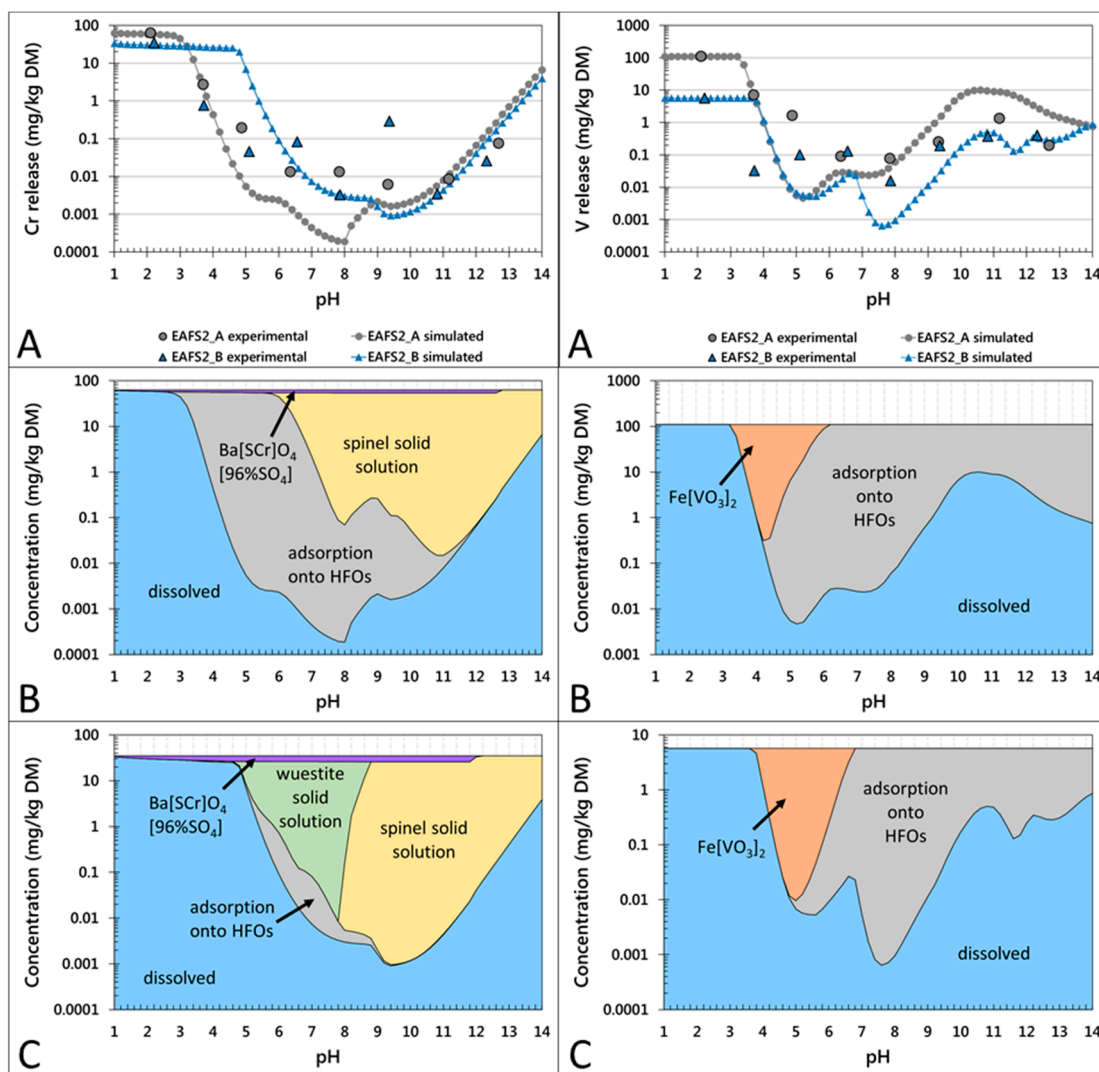


Figure 3. pH-dependent leaching behavior of Cr (left column) and V (right column) in the conditioned EAF slag samples EAFS2_A and EAFS2_B. Partitioning in the solution (A) and in the solid (B,C) are given on a weight basis. (A) Experimentally determined release of Cr and V, respectively (larger symbols without line) and calculated results with LeachXS™/Orchestra (corresponding symbols with lines). (B,C) Calculated concentrations of leaching control phases/mechanisms for Cr and V, respectively, in samples EAFS2_A (B) and EAFS2_B (C).

Table 4. Total content (tc) and leached amount at natural pH (in mg/kg DM and % of tc) for Cr and V as well as basicity (CaO/SiO₂), FeO/SiO₂ ratio, Al₂O₃, and MgO concentrations.

Parameter	EAFS1	EAFS2_1	EAFS2_2	EAFS2_A	EAFS2_B
Chromium					
Total content (mg/kg)	11,850	9775	9080	11,700	14,550
Leached amount at natural pH (mg/kg DM)	0.13	0.0065	0.0098	0.0084	0.0035
Leached amount at natural pH (% of tc)	1.10×10^{-3}	6.65×10^{-5}	1.08×10^{-4}	7.18×10^{-5}	2.41×10^{-5}
Vanadium					
Total content (mg/kg)	730	885	955	880	1085
Leached amount at natural pH (mg/kg DM)	2.5	1.5	2.4	1.3	0.37
Leached amount at natural pH (% of tc)	0.34	0.17	0.25	0.15	0.034
Ratio of total content/total content					
CaO/SiO ₂	2.03	2.31	2.74	1.21	0.94
FeO/SiO ₂	3.66	1.59	1.95	1.53	1.04
Al ₂ O ₃ (mass-%)	7.3	5.6	5.8	4.2	9.1
MgO (mass-%)	6.2	5.4	5.0	3.8	3.9
Leachate with distilled water (L/S = 10)					
Natural pH	11.2	11.1	11.2	11.2	10.8

3.4. Leached Concentrations and Chemical Composition.

By comparing the percentage of leached Cr and V at natural pH (10.8–11.2) relative to the total content (Table 4), it can be seen that the most significant difference evolved between the non-conditioned sample EAFS1 and the conditioned sample EAFS2_B (i.e., the samples showed two orders of magnitude difference in Cr leaching and one order of magnitude in V leaching).

The phase composition and the observed dissolution behavior after leaching for 48 h of both samples were similar (see Table 2 and Figure 1), however, the mineral phase distribution differed significantly (i.e., the wuestite to calcium silicate phase ratio). In EAFS1, wuestite was the main mineral phase, whereas in EAFS2_B, the calcium silicate phases were predominantly formed (Figure 1). Additionally, the Cr–spinel crystals in sample EAFS2_B were larger than those in sample EAFS1. Comparison of the bulk chemical composition with the leached amount revealed that a higher FeO/SiO₂ ratio correlated with higher V and Cr leaching (Table 4), with a Pearson correlation coefficient of 0.92 ($p < 0.05$) and 0.97 ($p < 0.01$), respectively. The basicity (CaO/SiO₂) of the samples and concentrations of elements, which are known to enhance the formation of spinel (e.g., MgO and Al₂O₃) showed weaker correlations and were not statistically significant at the 0.05 level for V and Cr leaching with Pearson correlation coefficients of 0.69, 0.84 and -0.26 for V and 0.19, 0.76, and 0.23 for Cr.

4. Discussion

4.1. Chromium

The incorporation of Cr in spinel and the stability of these phases prior to and after leaching was confirmed by the applied analytical methods (XRD, EMPA, and XANES) as well as by the hydrogeochemical model. Aside from the incorporation of Cr(III) in spinel, Cr is also bound in minor amounts in wuestite and in trace amounts in the olivine phases. The main controlling factor for the leaching of Cr is the formation of chromian spinel in the slag, which prevents the release of Cr into the environment, yielding a release below <0.15 mg/kg at natural pH.

The implementation of a spinel solid solution into the hydrogeochemical database, used for the applied model, yielded a good fit with the experimental data, supporting the hypothesis that spinels control the leaching of Cr in the pH range of approximately 8 to 13. However, the higher release of

Cr between pH 9 and 13 from slag sample EAFS1 when compared to all other slag samples could not be explained by the model, which underestimated the leaching behavior of Cr. Due to EMP analyses, which showed that Cr was also bound to wuestite, a wuestite solid solution with Cr_2O_3 as an end member was also implemented into the database. This did not affect the fit for sample EAFS1, but improved the fit for EAFS2_1 and EAFS2_2 in the natural pH range, where leaching was overestimated prior to the implementation of the wuestite solid solution. According to the model results, in most of the samples, except for sample EAFS2_A, the wuestite solid solution precipitated and bound Cr at a lower pH (4.5 to 5.5) or above pH 9–10. Nevertheless, the stability of wuestite at low pH values was not investigated experimentally because phase analyses by EMP was only performed with samples leached at natural pH. The precipitation of $\text{Ba}(\text{S,Cr})\text{O}_4(96\%\text{SO}_4)$, calculated by the model for all samples, would assume an oxidation of Cr(III) to Cr(VI) after leaching, although moderately oxidizing and reducing conditions were observed, respectively. Additionally, an oxidation reaction of Cr(III) to Cr(VI) was not confirmed analytically as neither the XANES measurements on single crystals prior to and after leaching [19], nor the chemical analyses after digestion of the leachates showed considerable concentrations of Cr(VI). These results indicate that the presence of $\text{Ba}(\text{S,Cr})\text{O}_4(96\%\text{SO}_4)$ is considered to be unlikely in the investigated slag samples.

In general, the extension of the database with solid solutions, which were identified by the mineralogical investigations, yielded good fits for the leaching of Cr from the described slag samples. Discrepancies between the modeled and experimental results may be based on the comparison of thermodynamic equilibrium calculations with a non-equilibrium system.

The study shows that the leaching behavior of Cr is influenced by the amount of spinel in which Cr is bound stably and in some samples (although the Cr concentrations are very low) by the incorporation of Cr in the olivine group phases, if these phases dissolve during leaching. No significant surface alterations for either spinel or wuestite were observed after leaching for 48 h (see SE-images, Figure 1), however, hydrogeochemical modeling of a simplified slag system (dissolved species: $\text{Fe}(\text{OH})^{4-}$, CrO_4^{2-} , Mg^{2+} , Mn^{2+} ; Figure S4) showed that the solubility of the spinel solid solution was almost one order of magnitude lower than that of the wuestite solid solution in the natural pH range. Therefore, it is assumed that a high abundance of spinel in addition to a low abundance of wuestite leads to low Cr release from EAF slags.

4.2. Vanadium

EMP analyses combined with XANES measurements [19] showed that V substitutes for cations in the B-position in the spinel structure, but is also incorporated in wuestite. Additionally, in one sample, V was bound in the olivines. EMP analyses of fresh and leached samples showed that the stability of the olivine depends on the amount of Mn, Fe, and Ca present in this phase: A higher amount of Mn and Fe and a correspondingly lower amount of Ca leads to a higher stability and subsequently to a reduced congruent V leaching. Congruent leaching from olivines was only observed in one sample. A possible Ca vanadate formation [18] as the secondary leaching control mechanism could not be investigated experimentally and was not supported by the applied geochemical model. Additionally, according to this hypothesis, sample EAFS2_1, where the olivine group phase dissolves after leaching, should leach less V than sample EAFS2_B, where neither the olivine nor the melilite group phases dissolved (Table 3 and Figure 1). Experiments showed that the opposite was the case and the lowest concentrations of V in all presented samples were detected in the leachate of sample EAFS2_B (Table 4).

In fact, by combining the gained experimental results with geochemical modeling in this study, a hypothesis was established where the leaching of V is controlled by the stable binding in spinel and by the potential adsorption onto hydrated mineral phases (e.g., calcium silicate hydrate (CSH) phases like melilite or (Fe, Mn bearing) olivine hydrates).

In contrast to Cr, where extending the database based on experimental results improved the model outcome, this approach did not show any effect for V. Although coulsonite (FeV_2O_4) was implemented into the database as an end member in the spinel solid solution and V_2O_4 and V_2O_5 (data for V_2O_3

are not available) in the wuestite solid solution, adsorption onto HFOs was the main controlling mechanism for the leaching of V, based on the modeled results. Experimental data of the amount of HFO was only available for two samples. Using this data as input for the model yielded a good agreement for sample EAFS2_1, but significantly overestimated the amount of adsorbing surface for sample EAFS1. Therefore, the amount of HFOs was fitted for every sample (except sample EAFS2_1), which resulted in a good fit of the shape of the modeled curve, but not for the concentration levels at natural pH. In addition to the HFO amount, the modeled adsorption curve strongly depends on the modeled Si curve, which itself is influenced by the Ca and Fe calculations. By decreasing the sum of p_e and pH to 10 and adjusting the CO_3^{2-} input for every sample, not only the fit for Fe and Ca, but also for Si and subsequently the fit for V was improved. This led to the assumption that the stability of the Fe bearing calcium silicate phases influences the adsorption capacity, meaning that due to the lower stability of the phase, more ions are released into the solution, which are more favorably adsorbed onto HFOs than V ions. As argued above, the dependence of the V leaching on the stability of calcium silicate phases is only of limited validity for the investigated samples because congruent leaching was only observed in one slag sample.

Nevertheless, the fact that the modeled and the experimental curve showed the same trend indicates that adsorption may influence the leaching of V. However, if the adsorption onto HFOs is the main controlling mechanism for the mobility of V, it could be expected that the sample, characterized by the highest concentrations of Fe (sample EAFS1) and additionally the highest amount of the presumably less stable phase wuestite (compared to spinel), would release the lowest V concentrations. The opposite was the case, where the highest concentration of V was leached from this sample at natural pH. Moreover, samples showing less V leaching contained a lower amount of Fe and wuestite, but a higher number of calcium silicate phases. Hence, the adsorption onto alternative secondary mineral surfaces might control the release of V. From the EMP analyses after leaching, it is assumed that the melilite group phases (end members, i.e., åkermanite and gehlenite) and Fe, Mn bearing olivines hydrate. The adsorption capacity of hydrated gehlenite was demonstrated by Dimitrova et al. [47], indicating that these phases may provide adsorbing surfaces in EAF slags instead of HFOs. Consequently, the leaching of V can be minimized by not only increasing the spinel formation, but also by decreasing the amount of wuestite in favor of increasing the amount of Fe bearing calcium silicate phases, which are hydrated during leaching and provide sorption sites for V.

4.3. Influence of FeO/SiO_2 and CaO/SiO_2 on the Release of Cr and V

Combining all experimental and modelled results, the following hypothesis can be proposed: both elements (Cr and V) are bound stably in spinels but may leach congruently from olivines, if these phases contain low amounts of Fe and Mn and high amounts of Ca. Additionally, melilites and Fe, Mn bearing olivines may hydrate during leaching and serve as potential adsorption surface for V. The formation of spinel, wuestite, and calcium silicate in the investigated EAF slags is influenced by the chemical composition of the slags, more precisely by the FeO/SiO_2 and CaO/SiO_2 ratio. In melts with low SiO_2 and high FeO content, the formation of wuestite is fostered, whereas the formation of silicate phases is less pronounced [48,49]. Higher SiO_2 concentrations therefore lead to lower quantities of wuestite and higher amounts of Fe bearing calcium silicate phases, which do not dissolve during leaching for 48 h, as shown in this study. Additionally, higher SiO_2 concentrations in the slag lead to a lower basicity (CaO/SiO_2 ratio). As described by Cabrera-Real et al. [30] more MgCr_2O_4 is formed at $\text{CaO}/\text{SiO}_2 = 1$ than at $\text{CaO}/\text{SiO}_2 = 2$ and higher MgO concentrations also support spinel formation. Comparison of the investigated EAF slags in this study, however, revealed only a weak positive correlation between Cr and V leaching and the MgO concentration in the slags. However, Cabrera-Real et al. [30] investigated a system without FeO, whereas in this study, slag samples contained up to 38 mass-% FeO. The influence of CaO/SiO_2 in the simplified system $\text{CaO}-\text{SiO}_2-\text{Fe}_2\text{O}_3-\text{MgO}$ is described by White [50], showing that at a ratio larger than 2:1 Fe_2O_3 is completely or partly bound to CaO, forming dicalcium ferrite,

whereas at a ratio below 2:1, Fe₂O₃ completely reacts with MgO to spinel. Similar relationships hold with FeO, Al₂O₃, and Cr₂O₃ present in the system.

Both described mechanisms are shown in sample EAFS1 with much higher amounts of FeO compared to SiO₂ (ratio = 3.66) and a basicity slightly above two (CaO/SiO₂ = 2.03). Therefore, more wuestite phases than Fe bearing calcium silicate phases formed and spinel formation was inhibited. Although the highest MgO concentrations were present in this sample, most of the MgO was consumed by the crystallization of the wuestite solid solution (Fe,Mg,Mn)O and spinel formation was additionally suppressed. This led to the highest leached concentrations of both V and Cr, of all investigated EAF slag samples because a high number of large wuestites was formed where only limited amounts of V and Cr could be incorporated and only a few and small spinels were formed, where V and Cr were bound stably. Additionally, hardly any hydrated melilites or Fe, Mn bearing olivines had formed, which would provide adsorption sites for V, if available. In contrast, slag sample EAFS2_B with the lowest ratio of FeO/SiO₂ (1.04) of all investigated slag samples and a CaO/SiO₂ ratio slightly below one (0.94) was characterized by numerous large crystals of Fe bearing calcium silicate phases, spinels, and a very small amount of small wuestite crystals. The MgO concentration was lower than in sample EAFS1, but MgO was not consumed by wuestite and was available for spinel formation. Thus, higher amounts of Cr and V could be bound in spinel and high amounts of potential adsorbing surfaces were available to additionally impede the leaching, as proven by the lowest observed concentrations of V and Cr in the leachates.

To achieve a low release of Cr and V from EAF slags, it is assumed that both the FeO/SiO₂ and CaO/SiO₂ ratios should be in the range of one.

5. Conclusions

Possible leaching control mechanisms for Cr and V from electric arc furnace slags were identified by combining experimental data and hydrogeochemical modeling results. Higher contents of spinel and Fe bearing calcium silicate phases and lower amounts of wuestite are supposed to reduce the release of Cr and V. The ratio of wuestite to Fe bearing calcium silicates and the abundance of spinel is controlled by the chemical composition (i.e., the FeO/SiO₂ and CaO/SiO₂ ratio present in the EAF slag). Therefore, minimized leaching of Cr and V may be achieved by adjusting the chemical composition, which controls the resulting mineral phase distribution. First conditioning experiments, where the FeO/SiO₂ (accompanied by the CaO/SiO₂) ratio of slag sample EAFS1 was modified in crucibles and in a pilot plant scale EAF, were conducted and show promising results.

Supplementary Materials: The following are available online at <http://www.mdpi.com/2075-163X/9/9/525/s1>, Figure S1: pH dependence leaching tests (experimental data and modeled results) for Ca, Si, Fe, Al, Mg, and Mn; Figure S2: X-ray diffraction pattern for sample EAFS1; Figure S3: Calculated leaching controlling phases and mechanisms of V (predominant and background species) for samples EAFS1, EAFS2_1, EAFS2_2, EAFS2_A, and EAFS2_B; Figure S4: Calculation of a simplified slag system using LeachXSTM; Tables S1–S14: Results of mineral chemical electron microprobe analyses for samples EAFS1, EAFS2_1, EAFS2_2, EAFS2_A, and EAFS2_B prior to and after leaching; Table S15: Input for estimated parameters via trial and error and the experimental data for HFO; Table S16: Implemented solid solutions; Table S17: Selected minerals; Tables S18–S22: Calculated leaching controlling phases and mechanisms for samples EAFS1, EAFS2_1, EAFS2_2, EAFS2_A, and EAFS2_B; Table S23: Phase list of sample EAFS1.

Author Contributions: Conceptualization, S.N., A.v.Z., P.D., D.M., S.S., T.G., J.G.R., R.P., and D.V.; Methodology, S.N., A.v.Z., H.A.v.d.S., J.J.D., P.D., D.A., D.M., S.S., T.G., J.G.R., R.P., and D.V.; Software, A.v.Z., H.A.v.d.S., J.J.D., S.N., and D.V.; Validation, S.N., A.v.Z., H.A.v.d.S., J.J.D., P.D., D.A., D.M., S.S., T.G., J.G.R., R.P., and D.V.; Formal analysis, S.N., A.v.Z., H.A.v.d.S., J.J.D., J.G.R., D.V., and P.D.; Investigation, S.N., D.V., and A.v.Z.; Resources, D.M., S.S., T.G., J.G.R., and A.v.Z.; Writing—original draft preparation, S.N.; Writing—review and editing, S.N., A.v.Z., H.A.v.d.S., J.J.D., P.D., D.A., D.M., S.S., T.G., J.G.R., R.P., and D.V.; Visualization, S.N.; Supervision, S.N., D.V., R.P., J.G.R., and A.v.Z.; Project administration, S.N. and D.V.; Funding acquisition, D.V., A.v.Z., P.D., D.M., S.S., T.G., J.G.R., and R.P.

Funding: This research was funded by the Austrian Research Promotion Agency (FFG), grant number 851210 in the program “Bridge Early Stage”, project MiLeSlag (Mineralogy and Leachability of Steel Slags).

Acknowledgments: The authors thank all participating project partners (Chair of Resource Mineralogy, Chair of Ferrous Metallurgy, Federal Institute for Materials Research and Testing, FEhS Building Materials Institute, ECN part of TNO, Max Aicher Umwelt GmbH, PORR Umwelttechnik GmbH, Scholz Austria GmbH and Stahl- und Walzwerk Marienhütte GmbH) for their contributions. Special thanks go to the laboratory staff and colleagues at the Chair of Waste Processing Technology and Waste Management and to Federica Zaccarini and Maik Zimmermann for the support during the electron microprobe analyses.

Conflicts of Interest: The authors declare no conflict of interest. The funders had no role in the design of the study; in the collection, analyses, or interpretation of data; in the writing of the manuscript, or in the decision to publish the results.

References

1. Schaffartzik, A.; Eisenmenger, N.; Krausmann, F.; Milota, E. *Ressourcennutzung in Österreich*; BMLFUW–Bundesministerium für Land- und Forstwirtschaft, Umwelt und Wasserwirtschaft (Lebensministerium): Vienna, Austria, 2015.
2. Bundesministerium für Nachhaltigkeit und Tourismus. *Die Bestandsaufnahme der Abfallwirtschaft in Österreich, Statusbericht 2019*; Bundesministerium für Nachhaltigkeit und Tourismus: Wien, Austria, 2019.
3. Perz, K. *Aufkommen, Verwertung und Behandlung von Abfällen in Österreich, Materialien zum Bundes-Abfallwirtschaftsplan 2001*; Umweltbundesamt GmbH: Klagenfurt, Austria, 2001.
4. Pasetto, M.; Baldo, N. Mix design and performance analysis of asphalt concretes with electric arc furnace slag. *Constr. Build. Mater.* **2011**, *25*, 3458–3468. [[CrossRef](#)]
5. Faleschini, F.; Brunelli, K.; Zanini, M.A.; Dabalà, M.; Pellegrino, C. Electric Arc Furnace Slag as Coarse Recycled Aggregate for Concrete Production. *J. Sustain. Metall.* **2016**, *2*, 44–50. [[CrossRef](#)]
6. Sas, W.; Głuchowski, A.; Radziemska, M.; Dzieciół, J.; Szymański, A. Environmental and geotechnical assessment of the steel slags as a material for road structure. *Materials* **2015**, *8*, 4857–4875. [[CrossRef](#)]
7. Ramezani-pour, A.A.; Nikravan, M.; Nadoushan, M.J. Study of the Mechanical Properties and Environmental Characteristics of Concrete with Electric Arc Furnace (EAF) Slag as Aggregates. In Proceedings of the 9th International Congress on Advances in Civil Engineering, Trabzon, Turkey, 27–30 September 2010.
8. Degner, M.; Fandrich, R.; Endemann, G.; Ghenda, J.T.; Letz, K.; Lungen, H.B.; Steller, I.; Wieland, H.J.; Winkhold, A.; Bartos, R.; et al. *Stahlfibel*; Verlag Stahleisen: Düsseldorf, Germany, 2009.
9. Alloway, B.J. *Schwermetalle in Böden*; Springer: Berlin/Heidelberg, Germany, 1995; ISBN 9783642635663.
10. Jaishankar, M.; Tseten, T.; Anbalagan, N.; Mathew, B.B.; Beeregowda, K.N. Toxicity, mechanism and health effects of some heavy metals. *Interdiscip. Toxicol.* **2014**, *7*, 60–72. [[CrossRef](#)]
11. Bencheikh-Latmani, R.; Obratsova, A.; Mackey, M.R.; Ellisman, M.H.; Tebo, B.M. Toxicity of Cr(III) to *Shewanella* sp. Strain MR-4 during Cr(VI) Reduction. *Environ. Sci. Technol.* **2007**, *41*, 214–220. [[CrossRef](#)]
12. Costa, M. Toxicity and Carcinogenicity of Cr(VI) in Animal Models and Humans. *Crit. Rev. Toxicol.* **1997**, *27*, 431–442. [[CrossRef](#)]
13. Leuschner, J.; Haschke, H.; Sturm, G. New investigations on acute toxicities of vanadium oxides. *Mon. Chem. Chem. Mon.* **1994**, *125*, 623–646. [[CrossRef](#)]
14. Domingo, J.L. Vanadium: A review of the reproductive and developmental toxicity. *Reprod. Toxicol.* **1996**, *10*, 175–182. [[CrossRef](#)]
15. Mukherjee, B.; Patra, B.; Mahapatra, S.; Banerjee, P.; Tiwari, A.; Chatterjee, M. Vanadium—An element of atypical biological significance. *Toxicol. Lett.* **2004**, *150*, 135–143. [[CrossRef](#)]
16. Chaurand, P.; Rose, J.; Domas, J.; Bottero, J.Y. Speciation of Cr and V within BOF steel slag reused in road constructions. *J. Geochem. Explor.* **2006**, *88*, 10–14. [[CrossRef](#)]
17. Chaurand, P.; Rose, J.; Briois, V.; Olivi, L.; Hazemann, J.L.; Proux, O.; Domas, J.; Bottero, J.Y. Environmental impacts of steel slag reused in road construction: A crystallographic and molecular (XANES) approach. *J. Hazard. Mater.* **2007**, *139*, 537–542. [[CrossRef](#)]
18. Hobson, A.J.; Stewart, D.I.; Bray, A.W.; Mortimer, R.J.G.; Mayes, W.M.; Rogerson, M.; Burke, I.T. Mechanism of Vanadium Leaching during Surface Weathering of Basic Oxygen Furnace Steel Slag Blocks: A Microfocus X-ray Absorption Spectroscopy and Electron Microscopy Study. *Environ. Sci. Technol.* **2017**, *51*, 7823–7830. [[CrossRef](#)]

19. Neuhold, S.; Höllen, D.; Pomberger, R.; Mudersbach, D.; Schüler, S.; van Zomeren, A. Influence of Leaching on the Surface of Steel Slags. In Proceedings of the Berliner Konferenz Mineralische Nebenprodukte und Abfälle, Berlin, Germany, 11–12 June 2018; TK Verlag: Berlin, Germany, 2018; pp. 250–264.
20. Weber, J.B. *Agrochemical Environmental Fate State of the Art*, 1st ed.; Leng, M.L., Leovey, E.M.K., Zubkoff, P.L., Eds.; Lewis Publishers: Uckfield, UK, 1995; ISBN 1-56670-034-5.
21. Dube, A.; Zbytniewski, R.; Kowalkowski, T.; Cukrowska, E.; Buszewski, B. Adsorption and Migration of Heavy Metals in Soil. *Polish J. Environ. Stud.* **2001**, *10*, 1–10.
22. Mudersbach, D.; Kuehn, M.; Geiseler, J.; Koch, K. Chromium Immobilisation in EAF-Slags from High-alloy Steelmaking: Tests at FEhS-Institute and Development of an Operational Slag Treatment Process. In Proceedings of the First Slag Valorisation Symposium, Leuven, Belgium, 6–7 April 2009; KU Leuven: Leuven, Belgium, 2009; pp. 101–110.
23. Aldrian, A.; Raith, J.G.; Höllen, D.; Pomberger, R. Influence of Chromium Containing Spinels in an Electric Arc Furnace Slag on the Leaching Behaviour. *J. Solid Waste Technol. Manag.* **2015**, *41*, 357–365. [[CrossRef](#)]
24. Strandkvist, I.; Engström, F.; Pålsson, K.; Björkman, B. The Influence of Iron Oxide on the Chromium Leachability of EAF Slag—A Full-Scale Study At Ovako Hofors. In Proceedings of the Scanmet IV: 4th International Conference on Process Development in Iron and Steelmaking, Luleå, Sweden, 10–13 June 2012; pp. 329–338.
25. Strandkvist, I.; Sandström, Å.; Engström, F. Effect of FeO/MgO Ratio on Dissolution and Leaching of Magnesiowüstite. *Steel Res. Int.* **2017**, *88*, 7. [[CrossRef](#)]
26. Mombelli, D.; Mapelli, C.; Barella, S.; Gruttadauria, A.; Saout, G.; Le Garcia-diaz, E. The efficiency of quartz addition on electric arc furnace (EAF) carbon steel slag stability. *J. Hazard. Mater.* **2014**, *279*, 586–596. [[CrossRef](#)]
27. Van Zomeren, A.; van der Laan, S.R.; Kobesen, H.B.A.; Huijgen, W.J.J.; Comans, R.N.J. Changes in mineralogical and leaching properties of converter steel slag resulting from accelerated carbonation at low CO₂ pressure. *Waste Manag.* **2011**, *31*, 2236–2244. [[CrossRef](#)]
28. Drissen, P. *Mineralische Bindung von Spurenelementen in Stahlwerksschlacken*; FEhS-Institut für Baustoff-Forschung e.V.: Duisburg, Germany, 2006.
29. Drissen, P. Binding of trace elements in steel slags. In Proceedings of the 5th European Slag Conference, Luxembourg, 19–21 September 2007; pp. 187–198.
30. Cabrera-Real, H.; Romero-Serrano, A.; Zeifert, B.; Hernandez-Ramirez, A.; Hallen-Lopez, M.; Cruz-Ramirez, A. Effect of MgO and CaO/SiO₂ on the immobilization of chromium in synthetic slags. *J. Mater. Cycles Waste Manag.* **2012**, *14*, 317–324. [[CrossRef](#)]
31. Mombelli, D.; Mapelli, C.; Barella, S.; Di Cecca, C.; Le Saout, G.; Garcia-diaz, E. The effect of chemical composition on the leaching behaviour of electric arc furnace (EAF) carbon steel slag during a standard leaching test. *J. Environ. Chem. Eng.* **2016**, *4*, 1050–1060. [[CrossRef](#)]
32. Loncnar, M.; van der Sloot, H.A.; Mladenović, A.; Zupančič, M.; Kopal, L.; Bukovec, P. Study of the leaching behaviour of ladle slags by means of leaching tests combined with geochemical modelling and mineralogical investigations. *J. Hazard. Mater.* **2016**, *317*, 147–157. [[CrossRef](#)]
33. Austrian Standards Institute. *ÖNORM S 2127:2011 Grundlegende Charakterisierung von Abfallhaufen oder von festen Abfällen aus Behältnissen und Transportfahrzeugen*; Austrian Standards Institute: Wien, Austria, 2011; p. 34.
34. Austrian Standards Institute. *ÖNORM EN 14346:2007 Charakterisierung von Abfällen—Berechnung der Trockenmasse durch Bestimmung des Trockenrückstandes oder des Wassergehaltes*; Austrian Standards Institute: Wien, Austria, 2007; p. 24.
35. Austrian Standards Institute. *ÖNORM EN 13656:2002 Charakterisierung von Abfällen—Aufschluss mittels Mikrowellengerät mit einem Gemisch aus Fluorwasserstoffsäure (HF), Salpetersäure (HNO₃) und Salzsäure (HCl) für die anschließende Bestimmung der Elemente im Abfall*; Austrian Standards Institute: Wien, Austria, 2002; p. 26.
36. Austrian Standards Institute. *ÖNORM EN ISO 17294-2:2005 Wasserbeschaffenheit—Anwendung der induktiv gekoppelten Plasma-Massenspektrometrie (ICP-MS)*; Austrian Standards Institute: Wien, Austria, 2005; p. 24.
37. Hafner, J. *Erarbeitung Eines Geeigneten Verfahrens zur Bestimmung von Fluor in Schlacken*; Montanuniversität Leoben: Leoben, Austria, 2017.

38. Deutsches Institut für Normung. *DIN 38405-24:1987 Deutsche Einheitsverfahren zur Wasser-, Abwasser- und Schlammuntersuchung—Anionen (Gruppe D)—Photometrische Bestimmung von Chrom(VI) mittels 1,5-Diphenylcarbazid (D24)*; Deutsches Institut für Normung: Berlin, German, 1987; p. 10.
39. Austrian Standards Institute. *ÖNORM EN 14429:2015 Charakterisierung von Abfällen—Untersuchung des Elutionsverhaltens—Einfluss des pH-Wertes auf die Elution unter vorheriger Säure/Base-Zugabe*; Austrian Standards Institute: Wien, Austria, 2015; p. 50.
40. Austrian Standards Institute. *ÖNORM S 2116-4:2001 Untersuchung verfestigter Abfälle: Elutionstest über 24 Stunden, 64 Tage, 2 Tage*; Austrian Standards Institute: Wien, Austria, 2001; p. 17.
41. Stumm, W.; Morgan, J.J. *Aquatic Chemistry*, 3rd ed.; John Wiley & Sons, Inc.: Mississauga, ON, Canada, 1996; ISBN 0-471-51184-6.
42. Kostka, J.E.; Luther, G.W. Partitioning and speciation of solid phase iron in saltmarsh sediments. *Geochim. Cosmochim. Acta* **1994**, *58*, 1701–1710. [[CrossRef](#)]
43. Blakemore, L.C.; Searle, P.L.; Daly, B.K. *Methods for Chemical Analysis of Soils*; Department of Scientific and Industrial Research: Lower Hutt, New Zealand, 1987.
44. Dzombak, D.A.; Morel, F.M.M. *Surface Complexation Modeling: Hydrous Ferric Oxides*; John Wiley & Sons, Inc.: Mississauga, ON, Canada, 1990; ISBN 0-471-63731-9.
45. Strunz, H.; Nickel, E. *Strunz Mineralogical Tables*, 9th ed.; Schweizerbart'sche Verlagsbuchhandlung: Stuttgart, Germany, 2001; ISBN 3-510-65188-X.
46. Rai, D.; Eary, L.E.; Zachara, J.M. Environmental chemistry of chromium. *Sci. Total Environ.* **1989**, *86*, 15–23. [[CrossRef](#)]
47. Dimitrova, S.V.; Mihailova, I.K.; Nikolov, V.S.; Mehandjiev, D.R. Adsorption capacity of modified metallurgical slags. In Proceedings of the IIIrd National Crystallographic Symposium, Singapore, 25 November–3 December 2012; pp. 30–36.
48. Blatt, H.; Tracey, R.J. *Petrology: Igneous, Sedimentary, and Metamorphic*, 2nd ed.; W. H. Freeman and Company: New York, NY, USA, 1996.
49. Dumm, J.Q.; Brown, P.W. Dissolution of iron in silicate melts. *J. Am. Ceram. Soc.* **1999**, *82*, 987–993. [[CrossRef](#)]
50. White, J. The Relationship of Phase Diagrams to Constitution and Microstructure in Ceramic and Ceramic-Metal System. In *Refractory Materials A Series of Monographs*; Margrave, J.L., Ed.; Academic Press: New York, NY, USA; London, UK, 1970; Volume 6, pp. 21–66.



© 2019 by the authors. Licensee MDPI, Basel, Switzerland. This article is an open access article distributed under the terms and conditions of the Creative Commons Attribution (CC BY) license (<http://creativecommons.org/licenses/by/4.0/>).